



OPEN

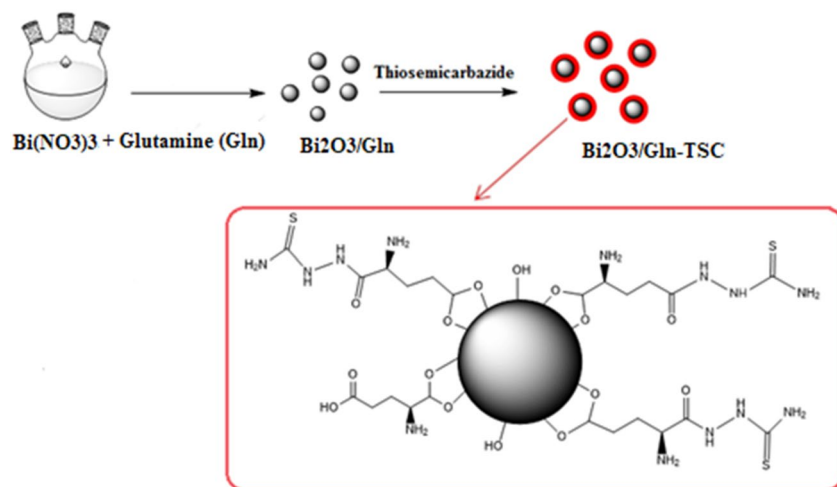
Synthesize of Bi₂O₃/Gln-TSC nanoparticles and evaluation of their toxicity on prostate cancer cells and expression of *CASP8*, *BAX*, and *Bcl-2* genes

Asal Moradi¹, Mohammadreza Abdihaji², Sara Barari Kouchaksaraie¹, Tabarek Abdulrazaq Alkinani³, Aida Mahmoudi⁴, Arash Davoudi^{1,5}, William Dashtmiani⁶, Somayeh Mikaeili Ghezeljeh¹, Shahrzad Aghajani¹, Reza Ghasemian⁷, Somayeh Maghsoomi Taramsari⁸, Amitis Majlesi¹, Zahra Mahdavi Niyaki¹ & Ali Salehzadeh¹✉

Due to the high prevalence and considerable increase of prostate cancer, finding novel therapeutic compounds for the treatment of prostatic cancer has been the goal of many researches. In this study, we aimed to fabricate the Bismuth oxide (Bi₂O₃) NPs, functionalized with glutamine (Gln) and conjugated with Thiosemicarbazide (TSC). Then, the anticancer mechanism of the synthesized NPs was investigated using the cellular and molecular tests including MTT assay, Flow cytometry, Caspase-3 activity assay, Hoechst staining and Real Time PCR. The FT-IR and XRD assays confirmed the identity of the synthesized Bi₂O₃/Gln-TSC NPs. The size range of the synthesized spherical particles was 10–60 nm and the zeta potential was – 23.8 mV. The purity of the NPs was confirmed by EDX-mapping analysis. The Bi₂O₃/Gln-TSC was considerably more toxic for prostate cancer cells than normal human cells and the IC₅₀ was calculated 35.4 and 305 µg/mL, respectively. The exposure to the NPs significantly increased the frequency of apoptotic cells from 4.7 to 75.3%. Moreover, the expression of the *CASP8*, *BAX*, and *Bcl-2* genes after exposure to the NPs increased by 2.8, 2.3, and 1.39 folds. Treating the cancer cells with Bi₂O₃/Gln-TSC increased the activity of the Caspase-3 protein and apoptotic morphological features were observed by Hoechst staining in the treated cells. This work showed that Bi₂O₃/Gln-TSC has considerable cytotoxicity for prostate cancer cells and could inducing both intrinsic and extrinsic pathways of apoptosis.

With an estimated 1,414,000 new cases, prostate cancer is considered the third most commonly diagnosed cancer, worldwide, after breast and lung cancers. This disease is involved with almost 375,000 deaths and is considered the 8th cause of cancer-associated death¹. The current therapeutic measures include chemotherapy, radiation, and surgery. Due to the lack of specificity, low efficacy, and considerable side-effects of conventional therapeutic methods, there has been an increasing interest in the application of nanotechnology for prostate cancer diagnosis and treatment². The large surface/volume ratio and morphology of the nanoparticles play a crucial role in their distribution in the body and their cytotoxic effect on cancer cells². Several nanostructures have been introduced for cancer treatment; however, controversial results have been observed³. The low efficacy and toxicity for normal cells are considered the most limiting factors in the development of many nanoparticles (NPs) in cancer

¹Department of Biology, Rasht Branch, Islamic Azad University, Rasht, Iran. ²Department of Biology, The Center for Genomics and Bioinformatics, Indiana University, Bloomington, IN, USA. ³Department of Biology, Science and Research Branch, Islamic Azad University, Tehran, Iran. ⁴Department of Biology, Damghan Branch, Islamic Azad University, Damghan, Iran. ⁵Division of Cytogenetic, Dr. Keshavarz Medical Genetics Lab, Rasht, Iran. ⁶Cancer Research Laboratories, Department of Surgery, St. George Hospital, University of New South Wales, Sydney, NSW 2217, Australia. ⁷Department of Medical Sciences, Faculty of Medicine, Tehran Medical Sciences, Islamic Azad University, Tehran, Iran. ⁸Max Perutz Labs, Vienna Biocenter (VBC), Dr. Bohr-Gasse 9, University of Vienna, Vienna, Austria. ✉email: salehzadeh@iaurasht.ac.ir



Scheme 1. Schematic diagram illustrating the synthetic procedure of $\text{Bi}_2\text{O}_3/\text{Gln-TSC}$ NPs.

treatment. Therefore, the preparation of novel nanostructures containing several effective molecules could be a promising method for the introduction of novel and safer anticancer agents for cancer treatment.

Bismuth NPs have gained considerable attention in the biomedicine and the cosmetic industry⁴. The bactericidal, fungicidal, antiparasitic and anti-biofilm properties of Bismuth NPs coated with lipophilic dimercapto-propanol NPs have been extensively studied in several papers^{5,6}. The in vitro cytotoxicity of Bismuth NPs coated with cellulose nanofibers was evaluated by MTT assay on mouse breast cancer cell lines⁷. Recently, Hamood et al.⁸ evaluated the anticancer activity of Bi@PVP NPs on the human MCF-7 breast cancer cell line. The cytotoxic effects of the BisBAL NPs were specifically studied on erythrocytes⁹, epithelial cells¹⁰, fibroblasts and cancer cells (cervical, prostate, colon in humans)¹¹. The generation of intracellular reactive oxygen species (ROS) and activation of cellular pro-apoptotic pathways have been the major cytotoxic features of these NPs that could be employed for cancer chemotherapy^{4–12}. However, the accumulation in the body and also, cytotoxic side effects are considered the major drawback of them to be used in medical applications.

Conjugation of therapeutic molecules is a novel approach that could be used to increase the efficacy of NPs in cancer treatment and reduce their cytotoxic side effects. Glutamine plays a critical role in cancer metabolism. An excessive uptake and consumption of glutamine by a variety of cancer cells have been reported^{13,14}. Therefore, conjugation of nanoparticles to glutamine may increase the efficacy of the complex molecule against cancer cells. Also, glutamine could be used for the functionalization of NPs and their conjugation to therapeutic molecules to increase their anticancer activity^{15,16}.

Thiosemicarbazides (TSCs) and their derivatives have shown considerable therapeutic potential as antiviral, antibacterial, and anticancer agents¹³. TSCs could interrupt the replication of cellular nucleic acids and inhibit cell proliferation¹⁴. Therefore, the conjugation of TSCs to NPs may increase the activity of the complex compared with either agent. In this regard, the present work aimed to fabricate bismuth oxide nanoparticle functionalized with glutamine and conjugated with TSC and to characterize its effect on prostate cancer cells and expression of *CASP8*, *BAX*, and *Bcl-2* genes.

Materials and methods

Synthesis of Bi_2O_3 and $\text{Bi}_2\text{O}_3/\text{Gln-TSC}$ NPs. To prepare $\text{Bi}_2\text{O}_3/\text{Gln}$ NP, at first, 300 mg of Bismuth (III) nitrate and 150 mg of Glutamine (Sigma-Aldrich) were dissolved in 150 mL of dissolved water and the pH was adjusted to 11.0 using 10% NaOH solution. Next, the mixture was heated at 80 °C for 2 h and the resulting dark pellet was harvested, washed, and dried at 70 °C for 8 h (Scheme 1).

For the synthesis of $\text{Bi}_2\text{O}_3/\text{Gln-TSC}$, 500 mg of the synthesized $\text{Bi}_2\text{O}_3/\text{Gln}$ and 200 mg of TSC were suspended in 150 mL 96% ethanol and sonicated for 45 min at 40 °C. The mixture was maintained at 40 °C for 24 h with continuous shaking. The prepared $\text{Bi}_2\text{O}_3/\text{Gln-TSC}$ NPs were harvested by centrifugation and dried at 70 °C for 8 h¹⁷.

Physicochemical assays were performed to characterize the prepared $\text{Bi}_2\text{O}_3/\text{Gln-TSC}$. FT-IR analysis was performed using a Nicolet IR 100 FT-IR spectrophotometer in a range of 500–4000 cm^{-1} . Also, the X-ray diffraction (XRD) pattern of the NP was determined to assess the crystalline structure of the particles (Co-K α X-radiation, $k=1.79$ Å). Scanning (Zeiss-Sigma VP, Germany) and transmission electron microscopy (Zeiss-EM10C, Germany) were used to determine the size range and morphology of the NP. The purity of the $\text{Bi}_2\text{O}_3/\text{Gln-TSC}$ was assessed using the EDX-mapping analysis. Further, Zeta potential and DLS analyses (Malvern Instruments Ltd, Ver. 6.32) were used to assess the stability and aggregation degree of the NP.

MTT assay. The PC3 prostate cancer cell line and HEK293 cell line (normal human cell line) were obtained from the National Cell Bank of Pasteur Institute of Iran. The cytotoxic effect of $\text{Bi}_2\text{O}_3/\text{Gln-TSC}$ on PC3 prostate cancer cells and HEK293 cells was evaluated by 2-(4,5-dimethylthiazol-2-yl)-2,5-diphenyltetrazolium bro-

Primer	Sequence (5'-3')	Product size (bp)	References
<i>BAX-forward</i>	TTGCTTCAGGGTTTCATCCA	113	34
<i>BAX-reverse</i>	AGACACTCGCTCAGCTTCTTG		
<i>CASP8-forward</i>	GACTGGATTGCTGATTACCTACCTAA	143	37
<i>CASP8-reverse</i>	CCTCAATTCTGATCTGCTCACTTCT		
<i>Bcl-2-forward</i>	TGGCCAGGGTCAGAGTAAA	147	34
<i>Bcl-2-reverse</i>	TGGCCTCTCTTGC GGAGTA		
<i>GAPDH-forward</i>	CCCCTCTCCACCTTTGAC	75	37
<i>GAPDH-reverse</i>	CATACCAGGAAATGAGCTTGACAA		

Table 1. Sequence of the primers used in this study (The efficiency of primers was provided in supplementary file).

mide (MTT) assay¹⁸. For culture maintenance, the cells were cultured on standard Dulbecco's modified Eagle's medium (DMEM) with 10% fetal bovine serum (FBS), 100 µg/mL streptomycin, and 100 units/mL penicillin solution at 37 °C in the presence of 5% humidified CO₂ in air. Approximately, 1 × 10⁴ cells were plated in each well of a 96-well plate and cultured for 24 h. Thereafter, the PC3 and HEK293 cells were exposed to a series of 15.6–500 µg/mL concentrations of Bi₂O₃/Gln-TSC at 37 °C in the presence of 5% humidified CO₂ for 24 h. The untreated cancer cells were assayed as control. After completion of incubation time, the untreated and Bi₂O₃/Gln-TSC treated cells were incubated by 100 µL MTT solution (0.5 mg/mL) at the same condition for 4 h. In each well, 100 µL of dimethyl sulfoxide (DMSO) was added to dissolve the formazan crystal formed in the reaction. The plate was shaken for 30 min and then, the optical absorbance at 590 nm was measured by a microplate ELISA reader instrument (Bio-Rad, Hercules, CA, USA). The ratios of OD value of treated Bi₂O₃/Gln-TSC samples to the untreated samples were used to calculate the percentage of cell viability. The following formula was used to calculate the 50% inhibitory concentration of the NP¹⁹:

$$\text{Growth inhibition\%} = 100 - \left[\frac{\text{Absorbance of sample}}{\text{Absorbance of control}} \times 100 \right] \quad (1)$$

Flow cytometry analysis. The PC3 cells were treated with Bi₂O₃/Gln-TSC NPs at IC₅₀ concentration. After 24 h incubation at 37 °C, the cells were washed and treated with propidium iodide and Annexin V (Roche, Germany). Then, flow cytometry analysis was performed (Partec flow cytometry device, Germany) to determine the frequency of apoptotic cells in NPs treated and control cells.

Quantitative PCR (qPCR). The effect of Bi₂O₃/Gln-TSC on the expression of *Bcl-2*, *BAX*, and *CASP8* genes in prostate cancer cells was investigated by SYBR green quantitative PCR assay. The cancer cells (about 5000 cells) were treated with the NPs at IC₅₀ concentration for 24 h, total RNA of the cells was extracted using the Tri-Zol reagent (Sigma-Aldrich), and cDNA was synthesized by SinaClone cDNA synthesis kit (Iran). The *GAPDH* gene was used as an internal reference gene. The sequence of the primers used in this study was presented in Table 1. Data analysis was performed according to the 2^{-ΔΔCT} method²⁰.

Activity of Caspase-3. The activity of Caspase-3 protein in Bi₂O₃/Gln-TSC treated and control cells was measured using the method described by Salehzadeh et al.²¹. After exposure of PC3 cells with IC₅₀ concentration of NP, the cells were lysed and the cell supernatant was treated with DEVD-pNA (CASP3C, Sigma-Aldrich). Finally, the optical density was measured at 405 nm.

Hoechst staining. To elucidate the nuclear damages, prostate cancer cells were treated with IC₅₀ concentration of Bi₂O₃/Gln-TSC NPs for 24 h. Then, the NPs treated and control cells were subjected to the Hoechst 33,258 solution for 5 min and examined under a fluorescent microscope¹⁸.

Statistical analyses. Significant differences between the NPs treated and control cells were assessed using the SPSS 16.0 software. One-way analysis of variance (ANOVA) along with Post hoc analysis according to Tukey's Test method was used to uncover specific differences between group means, when ANOVA test was significant. The assays were performed in triplicates and *p*-values less than 0.05 were considered statistically significant.

Results

Physicochemical features of NP. FT-IR analysis was performed to evaluate the functional groups of Bi₂O₃/Gln and Bi₂O₃/Gln-TSC NPs. The FT-IR spectra of Bi₂O₃/Gln revealed two peaks at 482 and 745 cm⁻¹ that are associated with the Bismuth atom. Also, the peaks observed at 1124, 1283, and 1383 cm⁻¹ contribute to the C-N, C-O, and CH₃ bonds. The peaks at 1635, 1729, and 3634 cm⁻¹ are associated with the N-H, O=C, and stretching O-H bonds, respectively²². Assessment of the FT-IR peaks of Bi₂O₃/Gln-TSC NPs indicated two peaks at 494 and 604 cm⁻¹ associated with the Bismuth atom, and three peaks at 743, 745, and 974 cm⁻¹ that are

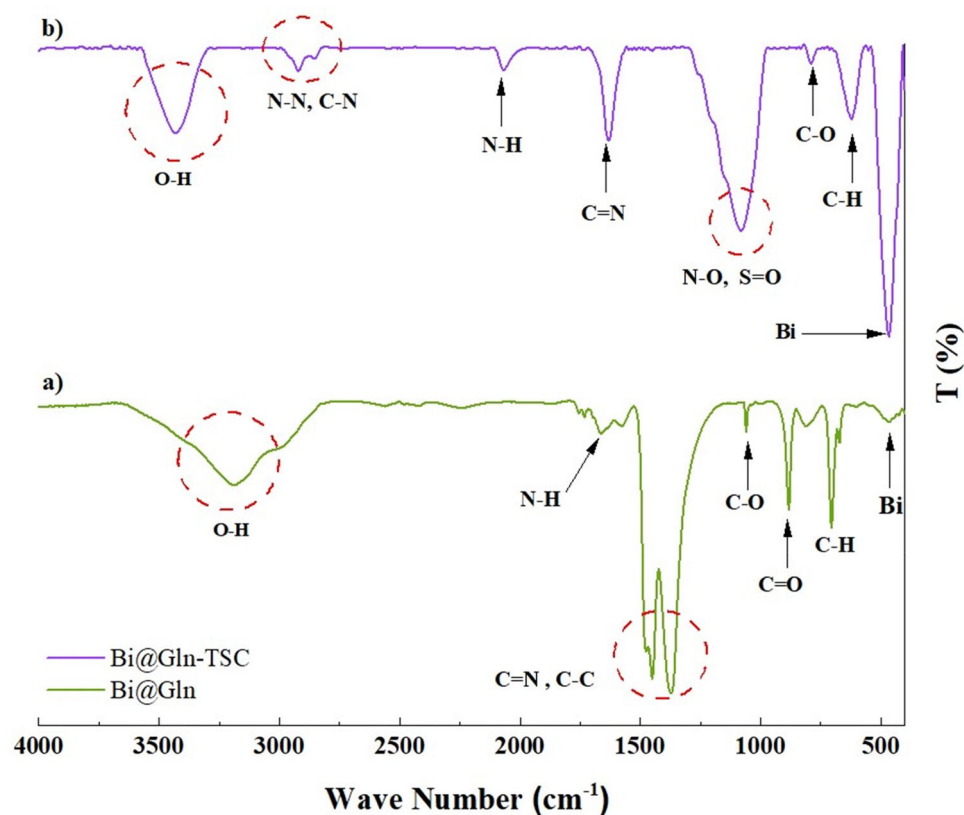


Figure 1. FT-IR analysis of (a) $\text{Bi}_2\text{O}_3/\text{Gln}$ and (b) $\text{Bi}_2\text{O}_3/\text{Gln-TSC}$ NPs.

associated with N–H, C–H, and N–H bonds, respectively. Also, the peaks at 1073, 1125, 1340, and 1384 cm^{-1} contribute to the C=S, C–N, C–O, and stretching N–O bonds, respectively. Moreover, the peaks at 1611, 1536, 1729, and 2096 cm^{-1} are associated with the N=O, C–C, C=N, and R–N=C=S bonds, respectively. The peak in the range of 3000–4000 cm^{-1} are associated with the O–H bond (Fig. 1).

Considering the XRD pattern of $\text{Bi}_2\text{O}_3/\text{Gln-TSC}$, the peaks at 2θ of 27.3 and 34° are associated with the Bismuth NP and comply with the JCPDS No. 01-058-1330²³. Also, the peaks that appeared at 2θ of 32, 35, and 55.2 contribute to the Glutamine molecule of the fabricated NPs²⁴. Considering the amorphous nature of TSC, two broad peaks at 2θ of 40 and 72, and also, the overall reduction of the peak intensity of $\text{Bi}_2\text{O}_3/\text{Gln-TSC}$ NPs (compared with the $\text{Bi}_2\text{O}_3/\text{Gln}$), the presence of TSC molecules could be concluded²⁵ (Fig. 2).

The SEM and TEM images of $\text{Bi}_2\text{O}_3/\text{Gln-TSC}$ NPs revealed that the synthesized NPs were almost spherical, with low aggregation, and with a size range of 10–60 nm. Figure 3 presents the electron microscopy images of the fabricated NPs. Moreover, the Zeta potential and hydrodynamic size of $\text{Bi}_2\text{O}_3/\text{Gln-TSC}$ were measured – 23.8 mV (Zeta SD = 14.7 mV) and 320 nm (PDI = 0.227), respectively that indicate the proper stability and low aggregation of the NPs. The results were displayed in Fig. 4. The EDX-mapping analysis revealed that the NPs contained Bi, C, N, O, and S atoms and were free of impurities (Fig. 5 and Table 2).

MTT assay. The cytotoxic effect of $\text{Bi}_2\text{O}_3/\text{Gln-TSC}$ for cancer cells and normal human cells was investigated by MTT assay. According to the results, the $\text{Bi}_2\text{O}_3/\text{Gln-TSC}$ NPs were more toxic for cancer cells than HEK293 cells with IC_{50} of 35.4 and 350 $\mu\text{g}/\text{mL}$, respectively. Furthermore, the IC_{50} of $\text{Bi}_2\text{O}_3/\text{Gln}$ NPs on cancer cell line was 74.8 $\mu\text{g}/\text{mL}$. Therefore, the cancer cells were considerably more susceptible to the synthesized NPs than normal human cells. Our results showed that at 6.25 $\mu\text{g}/\text{mL}$ and higher concentrations, $\text{Bi}_2\text{O}_3/\text{Gln-TSC}$ significantly reduced the viability of cancer cells. The results were presented in Fig. 6.

Flow cytometry analysis. Flow cytometry assay was performed to investigate the effect of exposure to $\text{Bi}_2\text{O}_3/\text{Gln-TSC}$ NPs on the apoptosis of prostate cancer cells. Our results showed that after exposure to the NPs, the frequency of apoptotic cells considerably increased compared with the control cells. The frequency of the cells with early and late apoptosis in control PC3 cells was measured 2.53 and 2.17%, respectively, while, after treating the cells with $\text{Bi}_2\text{O}_3/\text{Gln-TSC}$ NPs the frequency of early and late apoptosis increased to 19.6 and 55.7%, respectively. Also, about 2.54% of the treated cancer cells with NPs were in necrosis condition and 22.2% of them were alive. In treating the cancer cells with $\text{Bi}_2\text{O}_3/\text{Gln}$ NPs the frequency of early and late apoptosis was 28.57 and 5.51%, respectively. Furthermore, about 2.8% of the treated cancer cells with $\text{Bi}_2\text{O}_3/\text{Gln}$ NPs were in necrosis condition and 63.2% of them were alive. The results were presented in Fig. 7.

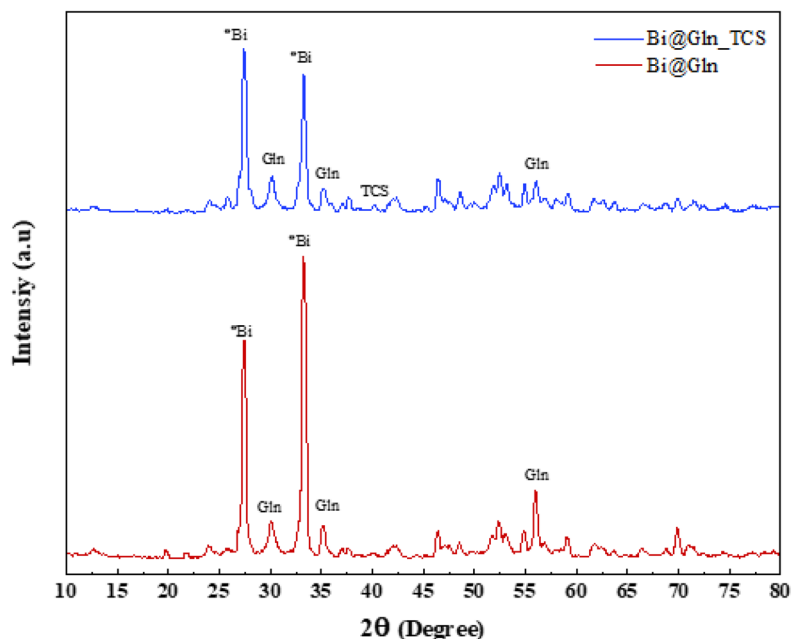


Figure 2. XRD pattern of the synthesized NPs.

Genes expression. The expression of the apoptosis pathway genes, including *BAX*, *Bcl-2* and *CASP8* genes in NPs treated and control PC3 cells was investigated. The qPCR assay showed that treating the cells with the NPs considerably up-regulated the *BAX* gene, with an increase of 2.3 folds. Also, the expression of the *Bcl-2* gene was slightly increased by 1.39 folds, after exposure to $\text{Bi}_2\text{O}_3/\text{Gln-TSC}$. The ratio of *BAX* to *Bcl-2* expression was equal to 1.65. The mRNA level of *CASP8* gene was also considerably increased by 2.8 folds in the treated cells, compared with the control PC3 cells. The results were displayed in Fig. 8.

Caspase-3 activity assay. The activity of caspase-3 protein in prostate cancer cells was significantly increased than in control cells. As presented in Fig. 9, we observed that the exposure to $\text{Bi}_2\text{O}_3/\text{Gln-TSC}$ could significantly increase the caspase-3 activity by 3.6 folds.

Hoechst staining. Hoechst staining assay was performed on the $\text{Bi}_2\text{O}_3/\text{Gln-TSC}$ treated and control cells to determine the possible nuclear damages caused from NPs exposure. The results revealed the chromatin condensation and fragmentation and also the appearance of apoptotic bodies as the major outcomes of exposure to $\text{Bi}_2\text{O}_3/\text{Gln-TSC}$ NPs (Fig. 10).

Discussion

The frequency of prostate cancer incidence and mortality has been increasing in recent years and thus, finding novel anticancer agents to treat this disease is the goal of many research projects¹. Nanotechnology products have received great attentions to be used in medicine, especially in cancer treatment. Due to the large surface area, nano-scale compounds could efficiently distribute in the host organs, reach their target sites and exert their cytotoxic effects on the target cells. However, the toxic side-effects of such compounds on the host's organs are the major barrier to their development and application of them in cancer chemotherapy. In this regard, the preparation of complex compounds containing different effective molecules could increase the efficiency and reduce undesirable features of nanotechnology products. In the current work, we aimed to prepare bismuth oxide NPs, functionalize them with glutamine, and conjugate it to TSC. Then, the effect of the $\text{Bi}_2\text{O}_3/\text{Gln-TSC}$ NPs on the viability and apoptosis pathway of prostate cancer cells was evaluated.

Identity of the fabricated $\text{Bi}_2\text{O}_3/\text{Gln-TSC}$ NPs were confirmed using the physicochemical assays. The FT-IR and XRD assays confirmed the proper functionalization and synthesis of the NPs. The zeta potential and XRD revealed the stability and low aggregation of the NPs. Further, the nano-scale size and purity of the NPs were confirmed by the electron microscopy and EDX-mapping analyses.

The MTT assay revealed that the fabricated $\text{Bi}_2\text{O}_3/\text{Gln-TSC}$ NPs were considerably more cytotoxic for the prostate cancer cells than normal human cells. Also, $\text{Bi}_2\text{O}_3/\text{Gln-TSC}$ NPs were more cytotoxic on cancer cell line than $\text{Bi}_2\text{O}_3/\text{Gln}$ NPs. Two main hypotheses could be introduced for the higher susceptibility of prostate cancer cells: (1) high proliferation rate and nutrient intake by cancer cells; (2) higher permeability of cancer cells. Due to the high proliferation rate, cancer cells have considerably higher membrane permeability than normal cells to accelerate cell nutrient intake²⁶. However, the increased cell permeability could facilitate the penetration of anticancer drugs into the cell. Moreover, glutamine, as an essential amino acid, is considered an essential nutrient for human cells. Due to the higher metabolic rate, cancer cells seem to have a higher demand for such

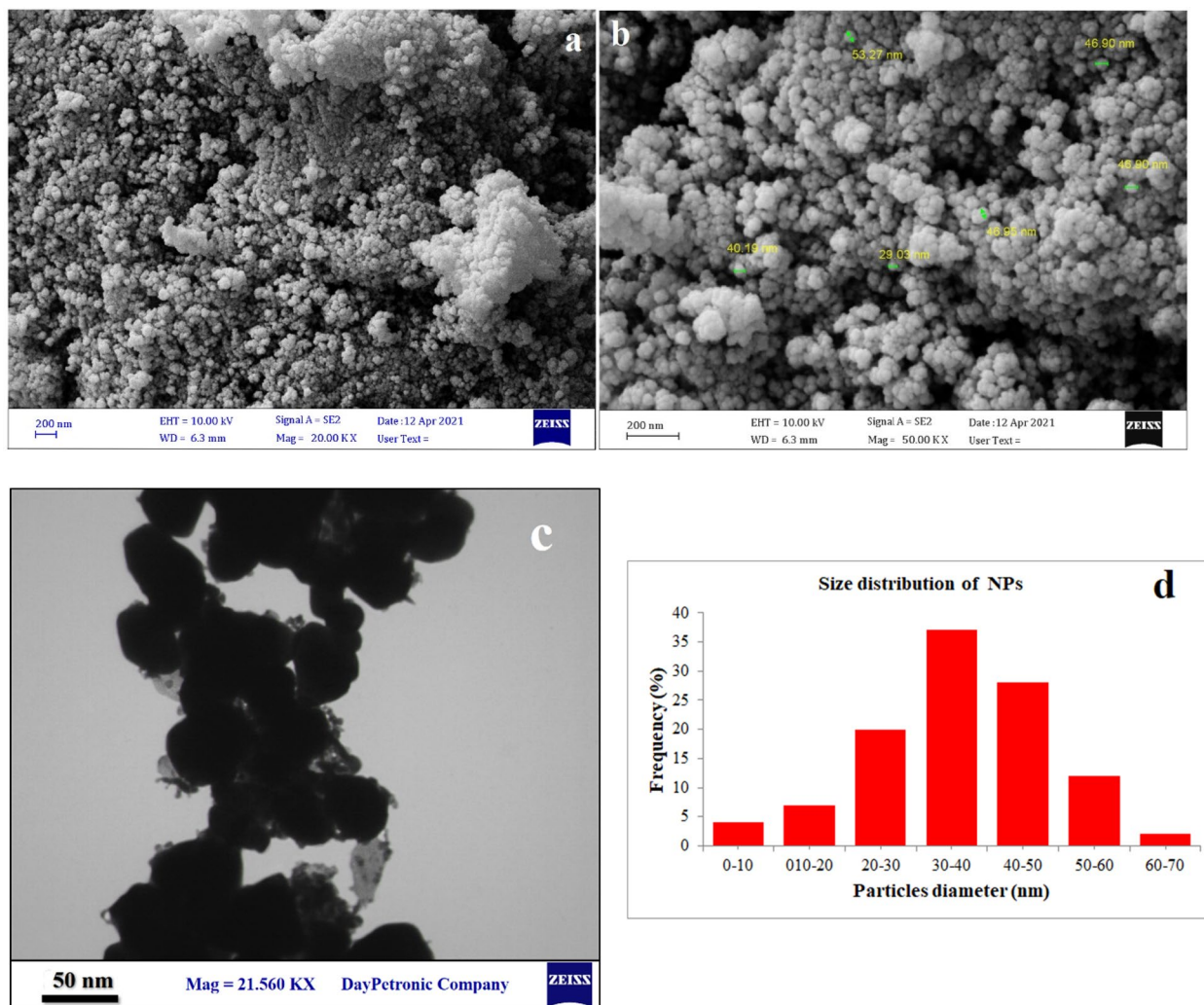


Figure 3. SEM (a,b), and TEM (c) images of $\text{Bi}_2\text{O}_3/\text{Gln-TSC}$ NPs. (d) Particle size distribution of synthesized NPs.

nutrients²⁷. The amino acid glutamine plays a key role in the metabolism of highly proliferating cells. During malignant transformation, cancer cells modify the consumption and processing of glutamine to sustain cell growth and proliferation. In some cases, these cancer cells become addicted to glutamine²⁸. Thus, targeting the metabolism of glutamine has been developed during last years as a potential strategy against cancer. Therefore, the higher susceptibility of prostate cancer cells than normal cells could be associated with the increased uptake of the $\text{Bi}_2\text{O}_3/\text{Gln-TSC}$ NPs into the cancer cells. Previous studies reported that exposure to bismuth NPs could generate radical oxygen species. The generated oxidative stress could damage major cell components, including cell membrane, nucleic acids, enzymes, etc. In addition, previous studies reported that TSC and its derivatives could interrupt the proliferation of eukaryote cells via the inhibition of the enzymes associated with nucleic acid synthesis and replication^{14,29,30}.

Evaluation of the frequency of apoptosis in the NP treated and control cells showed that $\text{Bi}_2\text{O}_3/\text{Gln-TSC}$ considerably increased the frequency of cell apoptosis. The increase of cell apoptosis suggests that $\text{Bi}_2\text{O}_3/\text{Gln-TSC}$ could arrest the cell cycle and initiate cell apoptosis. To investigate this hypothesis, the expression of the apoptotic genes and activity of Caspase-3 enzyme in NPs treated cells were investigated. Real-time PCR assay showed that the expression of *CASP8*, *Bcl-2*, and *BAX* genes in NPs treated cells were significantly increased, while exposure to the NPs downregulated the gene. Caspase-8 is an effector molecule in the extrinsic apoptotic signaling pathway. The generation of oxidative stress in the extracellular environment of NP s treated cells could result in the activation of Caspase-8 protein, which triggers the activation of apoptosis pathways via death receptors^{31,32}. Therefore, the increased expression of *CASP8* gene suggests the upregulation of the extrinsic apoptotic pathway that may be associated with the cytotoxic effects of the NPs. Also, the activity of Caspase-3 enzyme as the activator of the caspase-dependent apoptotic pathway was significantly increased upon exposure to $\text{Bi}_2\text{O}_3/\text{Gln-TSC}$ NPs³³. The increased activity of Caspase-3 enzyme reinforces the role of Caspases in the initiation of the apoptotic pathways in the NPs treated cells.

The expression of the *BAX* gene in NPs treated cells was increased significantly while exposure to $\text{Bi}_2\text{O}_3/\text{Gln-TSC}$ slightly increased the expression of *Bcl-2*. The BAX protein is regarded as a fundamental effector in

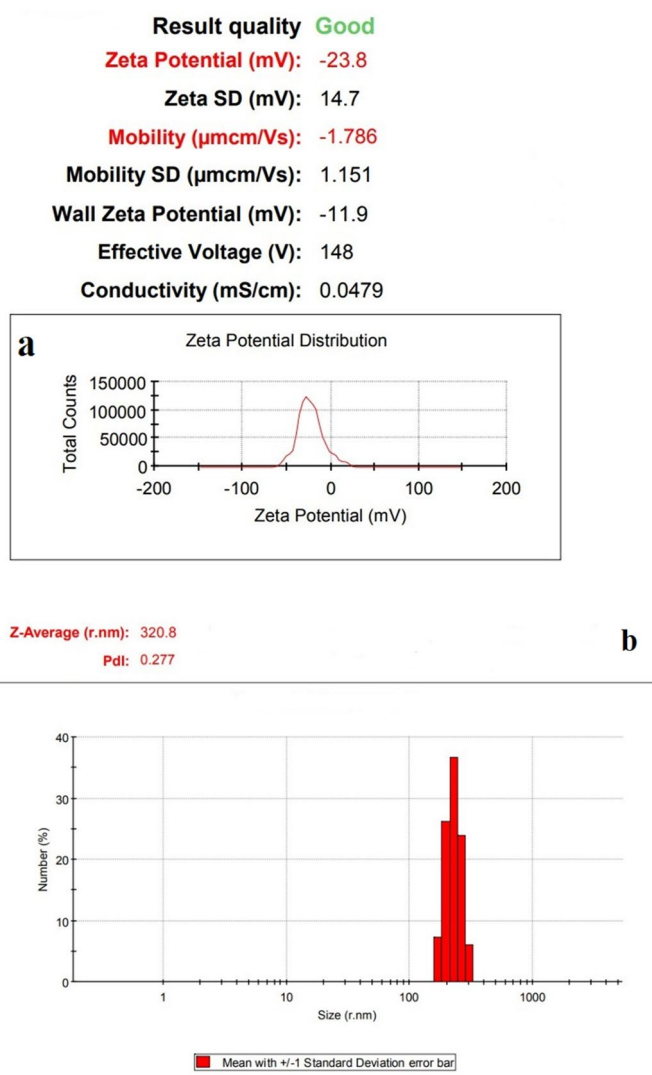


Figure 4. Zeta potential (a) and DLS (b) analyses of $\text{Bi}_2\text{O}_3/\text{Gln-TSC}$ NPs.

the intrinsic apoptosis signaling pathways³⁴. In contrast, the BCL2 protein mainly acts as the inhibitor of BAX molecules. The considerable increase of the *BAX/Bcl-2* ratio could suggest the activation of both intrinsic and extrinsic pathways of apoptosis in NPs treated cells. In accordance with the present results, previous studies have demonstrated that the *BAX/Bcl-2* ratio > 1 can induce the apoptosis^{35,36}.

The Hoechst staining of the cells after treatment with $\text{Bi}_2\text{O}_3/\text{Gln-TSC}$ NPs indicated the apoptosis features in the exposed cells. In agreement with the flow cytometry and molecular assays, the Hoechst staining confirmed the role of apoptosis in the death of prostate cancer cells in NPs exposed cells.

This work showed that $\text{Bi}_2\text{O}_3/\text{Gln-TSC}$ was highly effective against prostate cancer cells. The cytotoxic potential of $\text{Bi}_2\text{O}_3/\text{Gln-TSC}$ could be associated with synergism of all components, including Bi_2O_3 , glutamine, and TSC. As described above, cancer cells have high proliferation rate and nutrient uptake²⁶. Since glutamine is an essential nutrient for human cells, it may facilitate internalization of the $\text{Bi}_2\text{O}_3/\text{Gln-TSC}$ into the cancer cells²⁷. Inside the cells, other components, including Bi_2O_3 and TSC could exert their cytotoxic effects by generation of oxidative stress and inhibition of cell enzymes, respectively. Therefore, the synergistic effect of $\text{Bi}_2\text{O}_3/\text{Gln-TSC}$ components could induce apoptotic signaling pathways in prostate cancer cells.

Conclusion

In this study, $\text{Bi}_2\text{O}_3/\text{Gln-TSC}$ NPs were fabricated and its anticancer effect on prostate cancer cells was investigated. Our results revealed that the synthesized NPs were considerably more cytotoxic for cancer cells than normal human cells and the activation of cell apoptosis through both extrinsic and intrinsic pathways was suggested as the main cytotoxic mechanism of the NPs. Further investigations in in-vivo models could elucidate the potential of $\text{Bi}_2\text{O}_3/\text{Gln-TSC}$ NPs to be applied in anticancer chemotherapy.

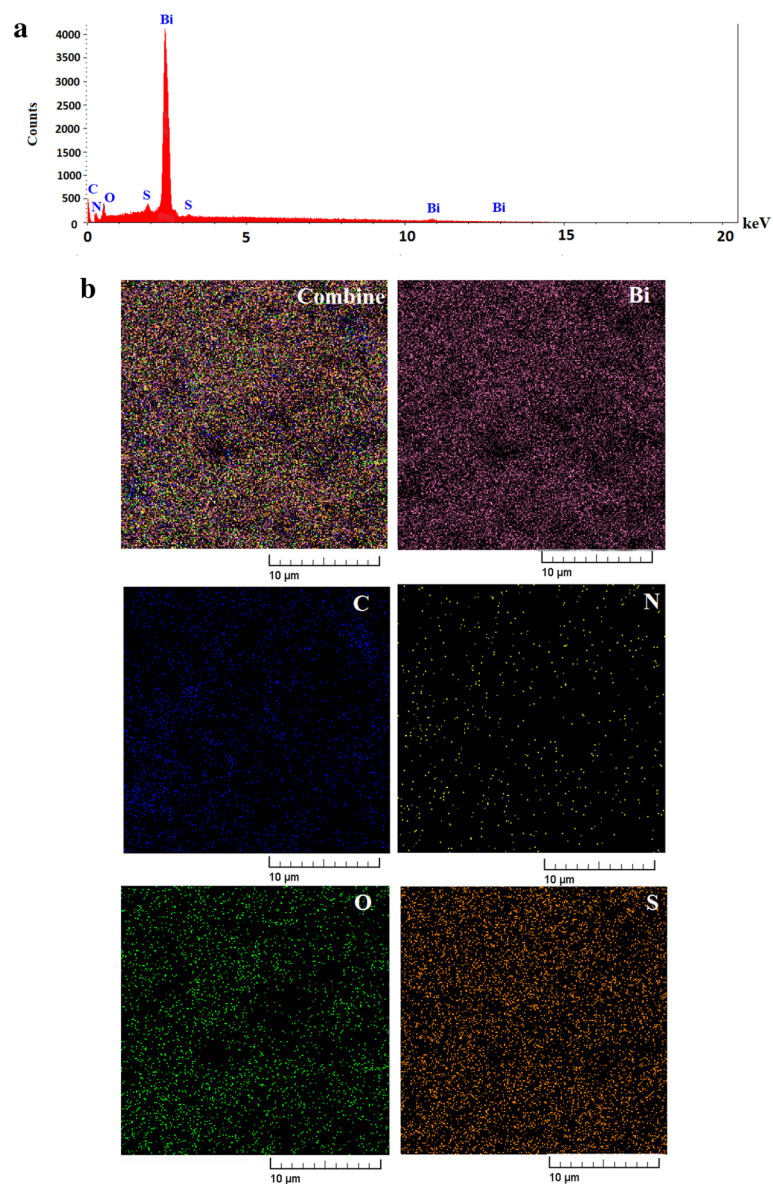


Figure 5. EDS-mapping of $\text{Bi}_2\text{O}_3/\text{Gln-TSC}$ NPs. The spectrum shows the presence of Bi, O, N, C and S elements in the final product ($\text{Bi}_2\text{O}_3/\text{Gln-TSC}$) (a). Also, the maps below the spectrum show the distribution of Bi, O, N, C and S elements in the final product (b).

Elements	Line	Int	Error	K	Kr	W%	A%	ZAF	Pk/Bg
C	Ka	65.7	151.1037	0.0211	0.0150	4.98	9.63	0.3005	74.93
N	Ka	33.5	151.1037	0.0108	0.0077	1.80	2.98	0.4283	29.67
O	Ka	1219.1	151.1037	0.3978	0.2824	46.28	67.20	0.6101	987.79
S	Ka	70.5	74.3259	0.0257	0.0182	2.14	1.55	0.8504	5.23
Bi	Ka	1207.2	0.6624	0.5446	0.3866	44.80	18.63	0.8630	44.23
				1.0000	0.7098	100.00	100.00		

Table 2. Elemental composition results of $\text{Bi}_2\text{O}_3/\text{Gln-TSC}$ NP in EDS-mapping analysis.

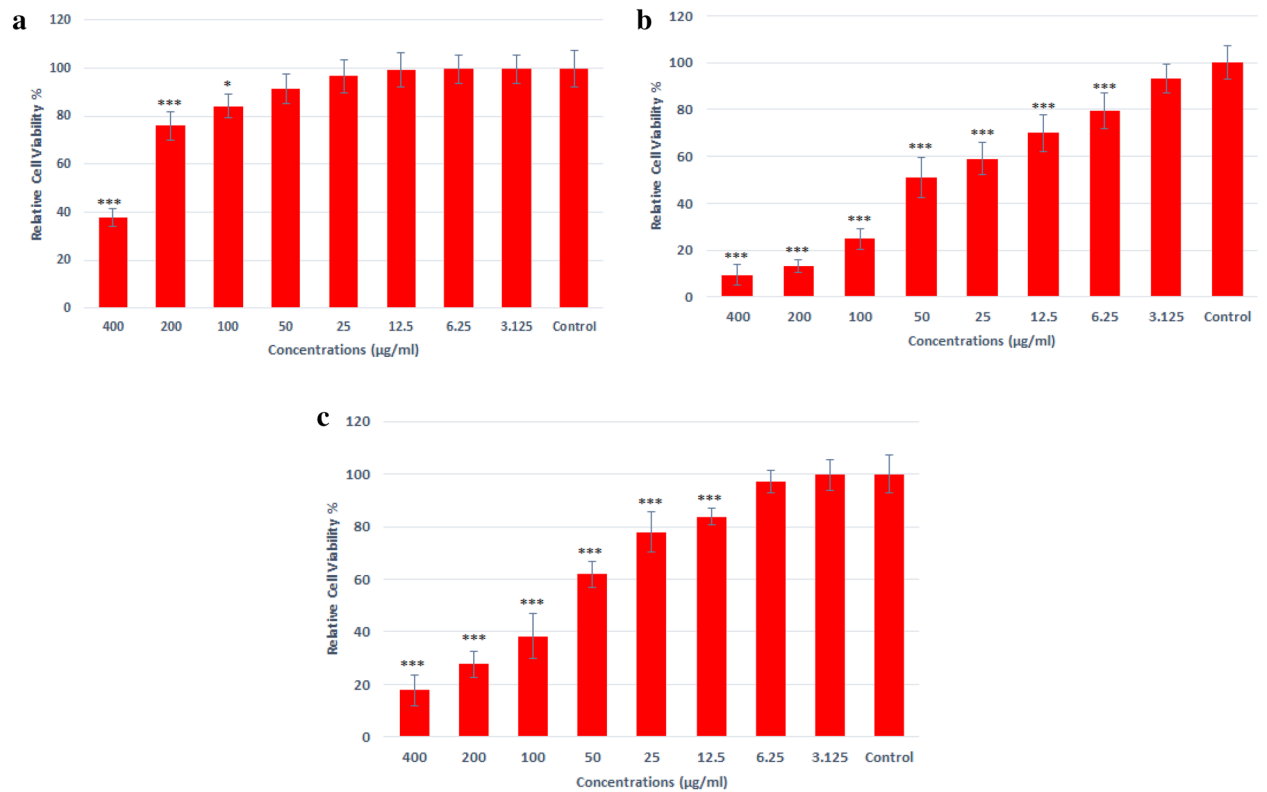


Figure 6. Viability of normal human cells (a) and prostate cancer cells (b) after treatment with $\text{Bi}_2\text{O}_3/\text{Gln-TSC}$ NPs c: Viability of prostate cancer cells after treatment with $\text{Bi}_2\text{O}_3/\text{Gln}$ NPs (Data are normalized to the untreated cells and reported as mean \pm SD. Asterisks (*) indicate a significant difference with the control group (* = $P < 0.05$, ** = $P < 0.01$, *** = $P < 0.001$).

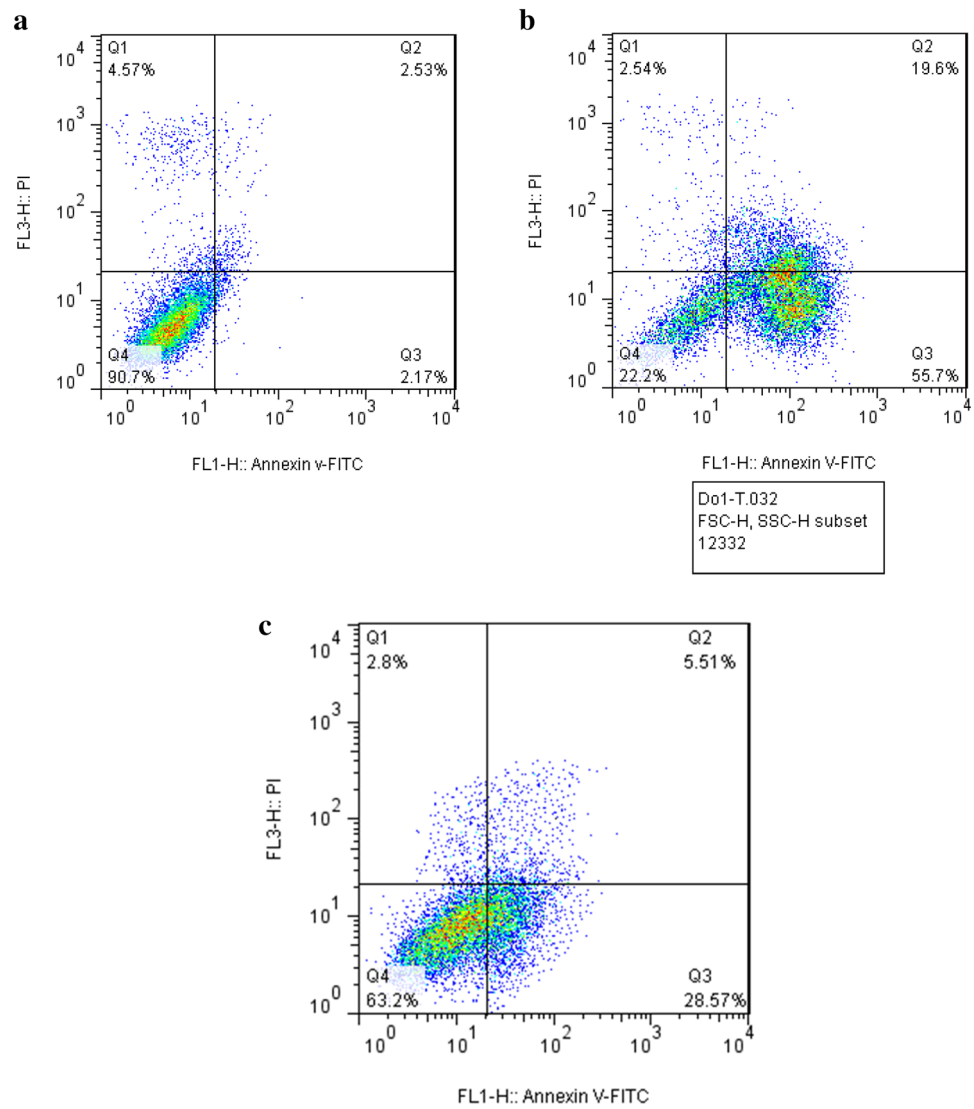


Figure 7. Flow cytometry of control (a), Bi₂O₃/Gln-TSC NPs treated cells (b) and Bi₂O₃/Gln NPs treated cells (c) (Q1: Necrotic cells, Q2: Late apoptosis, Q3: Early apoptosis, Q4: Live cells).

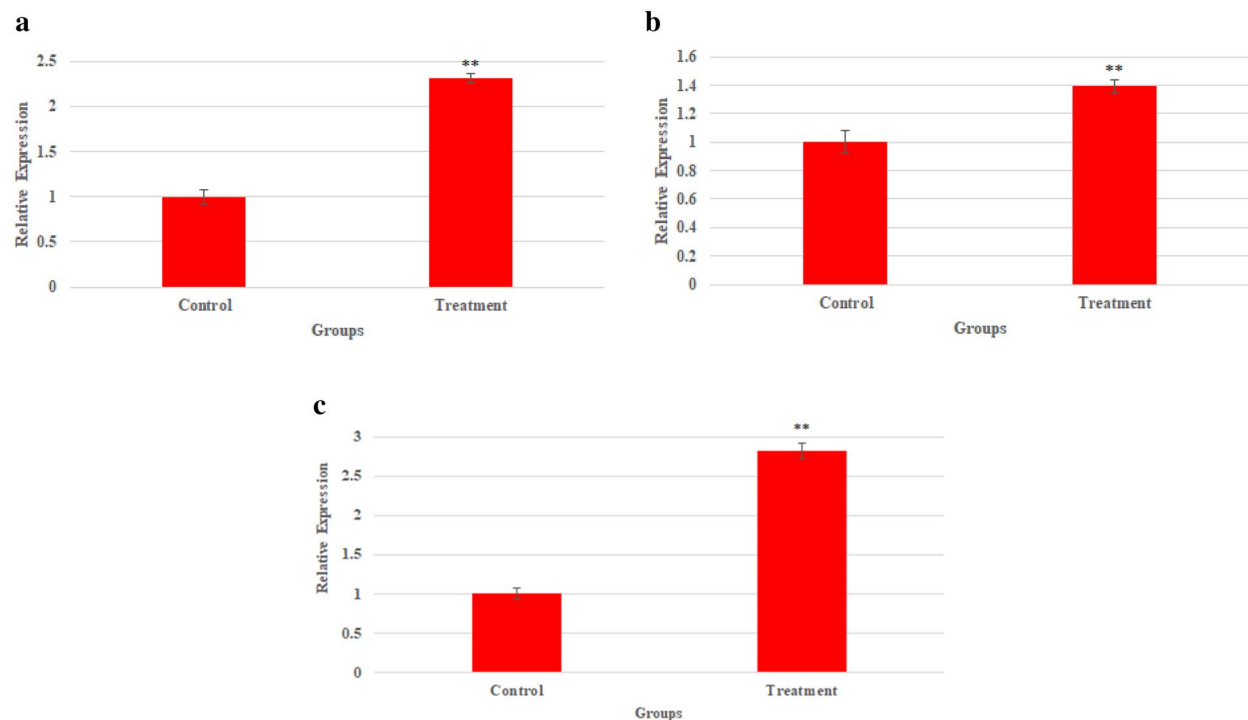


Figure 8. Relative expression of the (a) *BAX*, (b) *Bcl-2*, and (c) *CASP8* gene in $\text{Bi}_2\text{O}_3/\text{Gln-TSC}$ NPs treated cells. (Data are normalized to untreated cells and reported as mean \pm SD. Asterisks (*) indicate a significant difference with the control group (* = $P < 0.05$, ** = $P < 0.01$, *** = $P < 0.001$).

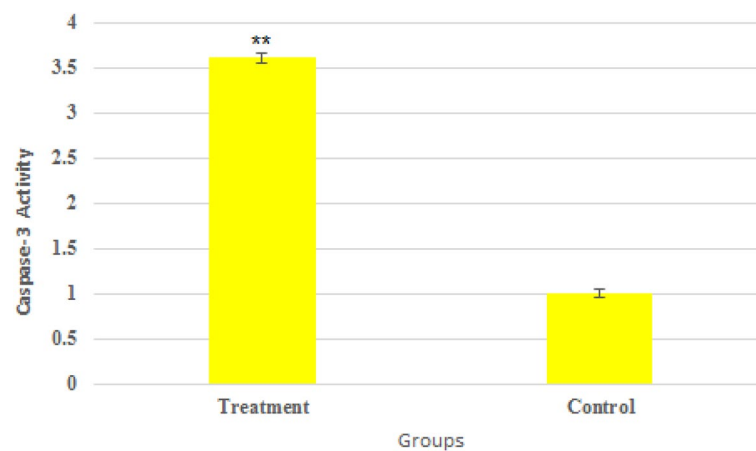


Figure 9. The activity of Caspase-3 enzyme in NPs treated and control cells. (Data are normalized to untreated cells and reported as mean \pm SD. Asterisks (*) indicate a significant difference with the control group (* = $P < 0.05$, ** = $P < 0.01$, *** = $P < 0.001$).

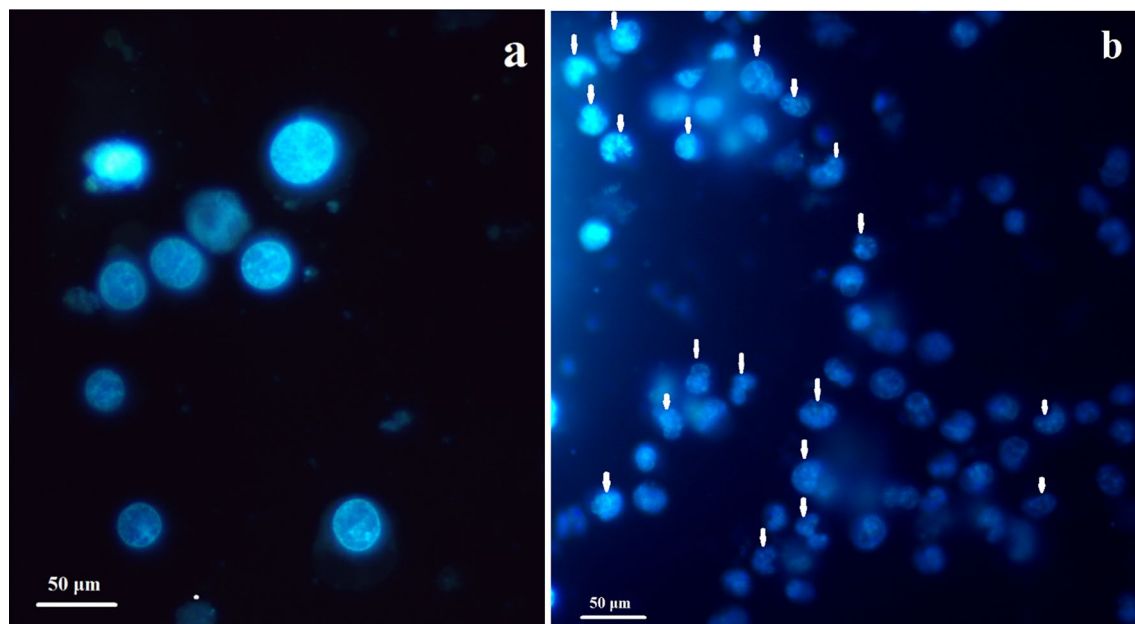


Figure 10. Hoechst staining of (a) control, and (b) $\text{Bi}_2\text{O}_3/\text{Gln-TSC}$ NPs treated cells. The arrows show the chromatin condensation and fragmentation and also the appearance of apoptotic bodies in the cells treated with $\text{Bi}_2\text{O}_3/\text{Gln-TSC}$ NPs.

Data availability

The datasets generated during the current study are available from the corresponding author on reasonable request.

Received: 9 September 2022; Accepted: 29 November 2022

Published online: 08 December 2022

References

- Sung, H. *et al.* Global cancer statistics 2020: GLOBOCAN estimates of incidence and mortality worldwide for 36 cancers in 185 countries. *CA Cancer J. Clin.* **71**(3), 209–249. <https://doi.org/10.3322/caac.21660> (2021).
- Sanna, V. & Sechi, M. Nanoparticle therapeutics for prostate cancer treatment. *Maturitas* **73**(1), 27–32. <https://doi.org/10.1016/j.maturitas.2012.01.016> (2012).
- Awasthi, R. *et al.* Nanoparticles in cancer treatment: Opportunities and obstacles. *Curr. Drug Targets* **19**(14), 1696–1709. <https://doi.org/10.2174/1389450119666180326122831> (2018).
- Alamer, A. *et al.* Bismuth oxide nanoparticles induce oxidative stress and apoptosis in human breast cancer cells. *Environ. Sci. Pollut. Res.* **28**(6), 7379–7389. <https://doi.org/10.1007/s11356-020-10913-x> (2021).
- Gomez, C., Hallot, G., Laurent, S. & Port, M. Medical applications of metallic bismuth nanoparticles. *Pharmaceutics* **13**(11), 1793. <https://doi.org/10.3390/pharmaceutics13111793> (2021).
- Azad, A., Rostamifar, S., Modaresi, F., Bazrafkan, A. & Rezaie, Z. Assessment of the antibacterial effects of bismuth nanoparticles against enterococcus faecalis. *Biomed. Res. Int.* <https://doi.org/10.1155/2020/5465439> (2020).
- Jiao, L. *et al.* Nanocellulose templated growth of ultra-small bismuth nanoparticles for enhanced radiation therapy. *Nanoscale* **10**(14), 6751–6757 (2018).
- Hamood, S. A. & Aldahan, Z. T. Novel biosynthesized gold nanoparticles as anti-cancer agents against breast cancer: Synthesis, biological evaluation, molecular modelling studies. *Mater. Sci. Eng., C Mater. Biol. Appl.* **99**, 417–429. <https://doi.org/10.1016/j.msec.2019.01.123> (2016).
- Hernandez-Delgado, R. *et al.* Effect of lipophilic bismuth nanoparticles on erythrocytes. *J. Nanomater.* **2015**, 264024. <https://doi.org/10.1155/2015/264024> (2015).
- Rene, H. D. *et al.* Cytotoxic effect of lipophilic bismuth dimercaptopropanol nanoparticles on epithelial cells. *J. Nanosci. Nanotechnol.* **16**(1), 203–209. <https://doi.org/10.1166/jnn.2016.10735> (2016).
- Cabral-Romero, C. *et al.* Antitumor activity of a hydrogel loaded with lipophilic bismuth nanoparticles on cervical, prostate, and colon human cancer cells. *Anticancer Drugs*. **31**(3), 251–259. <https://doi.org/10.1097/CAD.0000000000000863> (2020).
- Ahamed, M., Akhtar, M. J., Khan, M. M., Alrokayan, S. A. & Alhadlaq, H. A. Oxidative stress mediated cytotoxicity and apoptosis response of bismuth oxide (Bi_2O_3) nanoparticles in human breast cancer (MCF-7) cells. *Chemosphere* **216**, 823–831. <https://doi.org/10.1016/j.chemosphere.2018.10.214> (2019).
- Anjum, R. *et al.* Synthesis, characterization, and in vitro anticancer activity of copper and zinc bis (thiosemicarbazone) complexes. *Inorg. Chem.* **58**(20), 13709–13723. <https://doi.org/10.1021/acs.inorgchem.9b01281> (2019).
- Zaltariov, M. F. *et al.* New iminodiacetate–thiosemicarbazone hybrids and their copper (II) complexes are potential ribonucleotide reductase R2 inhibitors with high antiproliferative activity. *Inorg. Chem.* **56**(6), 3532–3549. <https://doi.org/10.1021/acs.inorgchem.6b03178> (2017).
- Buduru, P., Reddy, B. S. R. & Naidu, N. V. S. Functionalization of silver nanoparticles with glutamine and histidine for simple and selective detection of Hg^{2+} ion in water samples. *Sens. Actuat. B Chem.* **244**, 972–982. <https://doi.org/10.1016/j.snb.2017.01.041> (2017).

16. Elhambakhsh, A., Ghanaatian, A. & Keshavarz, P. Glutamine functionalized iron oxide nanoparticles for high-performance carbon dioxide absorption. *J. Natl. Gas Sci. Eng.* **94**, 104081. <https://doi.org/10.1016/j.jngse.2021.104081> (2021).
17. Abbaszadeh, N. *et al.* Preparation of novel nickel oxide@ glutamic/thiosemicarbazide nanoparticles: Implications for cytotoxic and anti-cancer studies in MCF-7 breast cancer cells. *J. Cluster Sci.* **33**, 457–465. <https://doi.org/10.1007/s10876-021-01995-9> (2021).
18. Hosseinkhah, M. *et al.* Cytotoxic potential of nickel oxide nanoparticles functionalized with glutamic acid and conjugated with thiosemicarbazide (NiO@ Glu/TSC) against human gastric cancer cells. *J. Cluster Sci.* <https://doi.org/10.1007/s10876-021-02124-2> (2021).
19. Zhao, Y. *et al.* A novel fluorinated thiosemicarbazone derivative-2-(3, 4-difluorobenzylidene) hydrazinecarbothioamide induces apoptosis in human A549 lung cancer cells via ROS-mediated mitochondria-dependent pathway. *Biochem. Biophys. Res. Commun.* **491**(1), 65–71. <https://doi.org/10.1016/j.bbrc.2017.07.042> (2017).
20. Pfaffl, M. W. A new mathematical model for relative quantification in real-time RT-PCR. *Nucleic Acids Res.* **29**, e45. <https://doi.org/10.1093/nar/29.9.e45> (2001).
21. Salehzadeh, A., Naeemi, A. S., Khaknezhad, L., Moradi-Shoeli, Z. & Shandiz, S. A. S. Fe₃O₄/Ag nanocomposite biosynthesized using *Spirulina platensis* extract and its enhanced anticancer efficiency. *IET Nanobiotechnol.* **13**(7), 766–770. <https://doi.org/10.1049/iet-nbt.2018.5364> (2019).
22. - Zulkifli, Z. A., Razak, K. A. & Rahman, W. N. W. A. The effect of reaction temperature on the particle size of bismuth oxide nanoparticles synthesized via hydrothermal method. In *AIP Conference Proceedings* (Vol. 1958, No. 1, p. 020007). AIP Publishing LLC. (2018).
23. Dadashi, S., Delavari, H. & Poursalehi, R. Optical properties and colloidal stability mechanism of bismuth nanoparticles prepared by Q-switched Nd: Yag laser ablation in liquid. *Procedia Mater. Sci.* **11**, 679–683 (2015).
24. Aghazadeh, M. *et al.* Facile electrosynthesis and characterization of superparamagnetic nanoparticles coated with cysteine, glycine and glutamine. *Appl. Phys. A* **123**(8), 1–10. <https://doi.org/10.1007/s00339-017-1145-5> (2017).
25. Yang, G. *et al.* Synthesis, characterization and antifungal activity of coumarin-functionalized chitosan derivatives. *Int. J. Biol. Macromol.* **106**, 179–184. <https://doi.org/10.1016/j.ijbiomac.2017.08.009> (2018).
26. Kettler, K., Veltman, K., van de Meent, D., van Wezel, A. & Hendriks, A. J. Cellular uptake of nanoparticles as determined by particle properties, experimental conditions, and cell type. *Environ. Toxicol. Chem.* **33**(3), 481–492. <https://doi.org/10.1002/etc.2470> (2014).
27. Wang, M. Preferential glutamine uptake in cancer cells. *Nat. Rev. Nephrol.* **17**(6), 368–368. <https://doi.org/10.1038/s41586-021-03442-1> (2021).
28. Halama, A. & Suhre, K. Advancing cancer treatment by targeting glutamine metabolism—a roadmap. *Cancers* **14**(3), 553. <https://doi.org/10.3390/cancers14030553> (2022).
29. Zeglis, B. M., Divilov, V. & Lewis, J. S. Role of metalation in the topoisomerase II α inhibition and antiproliferation activity of a series of α -heterocyclic-N4-substituted thiosemicarbazones and their Cu (II) complexes. *J. Med. Chem.* **54**(7), 2391–2398. <https://doi.org/10.1021/jm101532u> (2011).
30. Qi, J. *et al.* Pyridoxal hydrochloride thiosemicarbazones with copper ions inhibit cell division via Topo-I and Topo-II α . *J. Inorg. Biochem.* **232**, 111816. <https://doi.org/10.1016/j.jinorgbio.2022.111816> (2022).
31. Pozzesi, N. *et al.* Role of caspase-8 in thymus function. *Cell Death Differ.* **21**(2), 226–233. <https://doi.org/10.1038/cdd.2013.166> (2014).
32. Kominami, K. *et al.* The molecular mechanism of apoptosis upon caspase-8 activation: Quantitative experimental validation of a mathematical model. *Biochimica et Biophysica Acta (BBA) Mol. Cell Res.* **1823**(10), 1825–1840. <https://doi.org/10.1016/j.bbamcr.2012.07.003> (2012).
33. Peña-Blanco, A. & García-Sáez, A. J. Bax, Bak and beyond—mitochondrial performance in apoptosis. *FEBS J.* **285**(3), 416–431. <https://doi.org/10.1111/febs.14186> (2018).
34. Xu, Y. *et al.* CCL21/CCR7 prevents apoptosis via the ERK pathway in human non-small cell lung cancer cells. *PLoS ONE* **7**(3), e33262. <https://doi.org/10.1371/journal.pone.0033262> (2012).
35. Raisova, M. *et al.* The Bax/Bcl-2 ratio determines the susceptibility of human melanoma cells to CD95/Fas-mediated apoptosis. *J. Invest. Dermatol.* **117**(2), 333–340. <https://doi.org/10.1046/j.0022-202x.2001.01409.x> (2001).
36. Figueiredo, J. C. *et al.* Proliferation, apoptosis and their regulatory protein expression in colorectal adenomas and serrated lesions. *PLoS ONE* **16**(11), e0258878. <https://doi.org/10.1371/journal.pone.0258878> (2021).
37. Bigdeli, R. *et al.* Cytotoxic and apoptotic properties of silver chloride nanoparticles synthesized using *Escherichia coli* cell-free supernatant on human breast cancer MCF 7 cell line. *Artif. Cells Nanomed. Biotechnol.* **47**(1), 1603–1609. <https://doi.org/10.1080/21691401.2019.1604533> (2019).

Acknowledgements

The authors would like to thank to Dr. Akram Sadat Naeemi from university of Guilan for her help and support.

Author contributions

Conceptualization: A.M., M.R.A., S.B.K., T.A.A., A.M., A.S.; Methodology: A.D., W.D., S.M.G.H., A.S.; Formal analysis and investigation: S.H., A.G., R.G.H., Z.M.N., S.M.T., A.S.; Writing Original Draft Preparation: A.S.; Editing: A.M., Z.M.N., S.H.A.G.; Resources: A.M., M.R.A., S.B.K., T.A.A., A.M., Z.M.N., S.H.A.G.; Supervision: A.S.

Competing interests

The authors declare no competing interests.

Supplementary information

Supplementary Information The online version contains supplementary material available at <https://doi.org/10.1038/s41598-022-25360-6>.

Correspondence and requests for materials should be addressed to A.S.

Reprints and permissions information is available at www.nature.com/reprints.

Publisher's note Springer Nature remains neutral with regard to jurisdictional claims in published maps and institutional affiliations.



Open Access This article is licensed under a Creative Commons Attribution 4.0 International License, which permits use, sharing, adaptation, distribution and reproduction in any medium or format, as long as you give appropriate credit to the original author(s) and the source, provide a link to the Creative Commons licence, and indicate if changes were made. The images or other third party material in this article are included in the article's Creative Commons licence, unless indicated otherwise in a credit line to the material. If material is not included in the article's Creative Commons licence and your intended use is not permitted by statutory regulation or exceeds the permitted use, you will need to obtain permission directly from the copyright holder. To view a copy of this licence, visit <http://creativecommons.org/licenses/by/4.0/>.

© The Author(s) 2022